RSC Advances

ROYAL SOCIETY OF CHEMISTRY

www.rsc.org/advances

Journal Name

ARTICLE

Size-controlled synthesis of water-dispersible superparamagnetic Fe_3O_4 nanoclusters and their magnetic responsiveness†

Received 00th January 20xx,
Accepted 00th January 20xx

DOI: 10.1039/x0xx00000x

www.rsc.org/advances

Wentao Wang, Bingtao Tang,* Benzhi Ju and Shufen Zhang

Highly water dispersible and size-controllable superparamagnetic Fe_3O_4 nanoclusters were synthesized by simple solvothermal route with sodium citrate as surface modifier in a mixed-solvent system with diethylene glycol (DEG) and ethylene glycol (EG). The Fe_3O_4 nanoclusters are small-molecule grafted and the size of Fe_3O_4 nanoclusters can be effectively controlled by varying the volume ratio of DEG/EG from tens to hundreds of nanometers. Sodium citrate did not only act as functional ligand anchor on the particle surface to enhance the dispersibility of the magnetite nanoclusters but also controlled the size of the clusters in the reaction. Magnetic measurements revealed the superparamagnetic nature of the magnetic nanoclusters with no coercivity and remanence but with a magnetization saturation of up to 68.0 emu·g^{-1} at room temperature. These monodisperse Fe_3O_4 nanoclusters can be used for color display and hyperthermia in biomedical applications because of strong magnetic responsiveness. The diffraction color in the visible light can be modulated under the induction of varied external magnetic fields. Furthermore, the temperature of 20 mg·mL^{-1} Fe_3O_4 (168 nm) water dispersions can be increased by 46.7 °C within 242 s under alternating current magnetic field.

Introduction

Nanostructured magnetic particles have received extensive attention in the past decades because of their intriguing properties and potential applications in high-density magnetic recording media,[1,2] catalysts,[3-5] magnetic resonance imaging (MRI),[6-10] drug delivery technology,[11-13] and lithium-ion batteries.[14-16] Among these magnetic nanoparticles, superparamagnetic Fe_3O_4 nanoparticles have been considered ideal candidates for optics and biological applications because of their excellent magnetic field responsiveness, biological compatibility, chemical stability, and low toxicity.[17-23] For instance, Yin et al. developed a magnetically induced self-assembly of colloidal photonic crystals by using Fe_3O_4 colloidal nanocrystal clusters.[24] Sangregorio et al. designed a magnetic fluid hyperthermia heat mediator for the human body by coating Fe_3O_4 magnetic nanoparticles with sugar.[25] To attain reliable and high performance in optics and biomedical applications, magnetic particles with regular spherical shape (for chain-like photonic crystals self-assembling[21,26] and function molecules binding[27-29]), narrow size distributions, high-saturation magnetization for rapid magnetic response to externally applied magnetic fields, and good dispersion in liquid media for stability in physiological conditions is very important.[30] Therefore, the synthesis of monodispersed, water-dispersible, and regular spherical Fe_3O_4 nanoclusters with tunable sizes and excellent magnetic properties will be of great importance.

To address the above problems, many scientists have conducted substantial research in the past few years. Li et al. reported a convenient synthesis of hydrophilic magnetite nanospheres by a solvothermal reaction via reduction of $FeCl_3$ with EG in the presence of polyethylene glycol (PEG),[31] but the resultant magnetic nanospheres were ferromagnetic and not water-dispersible.[30] Moreover, the spherically uniform Fe_3O_4 spheres synthesized by this method have been limited to diameters larger than 200 nm. Wang et al. also reported the morphology-controllable synthesis of monodisperse Fe_3O_4 microspheres capped by polyvinylpyrrolidone (PVP) molecules with the average size of about 150 nm in a hydrothermal process.[1] However, the product also showed ferromagnetic behavior and low-saturation magnetization. Recently, Yin et al. reported a high-temperature hydrolysis method to grow poly(acrylic acid) (PAA) modified monodisperse Fe_3O_4 nanoclusters by injecting hot NaOH/DEG stock solution into a high-temperature mixture of DEG, $FeCl_3$, and PAA.[32] These as-prepared Fe_3O_4 particles can be assembled to photonic crystals in aqueous solution upon an externally applied magnetic field.[24] However, this method was based on complex multistep reactions with low efficiency and yield.[33] More recently, Xuan et al. used the bi-solvent system to synthesis Fe_3O_4 particals using Na acrylate, PAA , and PVP as the stabilizer.[34] All of these stabilizers mentioned above formed high polymers bonded on the surface of Fe_3O_4 particles.

State Key Laboratory of Fine Chemicals, Dalian University of Technology, Dalian 116024, China. E-mail : tangbt@dlut.edu.cn; Fax: +86-411-84986264; Tel: +86-411-84986267

† Electronic Supplementary Information (ESI) available: TEM and HRTEM images of Fe_3O_4 particles synthesized with 80/0 of V_{DEG}/V_{EG}, SEM images of Fe_3O_4 particles synthesized without Na3Cit and with 0.1 g Na_3Cit, hydrodynamic size and PDI at different pHs, a typical intensity particle size distribution at pH=7, FTIR spectra of Fe_3O_4 nanoparticles, reflection spectra of the photonic crystals. See DOI: 10.1039/x0xx00000x

In the present study, we report the synthesis of highly water-dispersible and size-controllable superparamagnetic Fe_3O_4 nanoclusters by using sodium citrate with a mixed-solvent system of DEG/EG via one-pot solvothermal method. The Fe_3O_4 nanoclusters are small-molecule grafted and the sizes of Fe_3O_4 nanoclusters can be effectively adjusted by varying the volume ratio of DEG/EG in our experiment. Compared with PEG and PVP, sodium citrate contains three carboxylate ions ($–COO^-$), which enable the highly water-dispersible Fe_3O_4 nanoclusters for the $–COO^-$ to strongly coordinate with Fe atom of Fe_3O_4 nanocrystals[35] and the uncoordinated $–COO^-$ extend to aqueous solution, producing a high degree of dispersibility by the electrostatic repulsion between the nanocrystals. Moreover, in comparison to PAA, sodium citrate is totally non-toxic and widely existing in vivo, thereby benefiting Fe_3O_4 nanoclusters as promising materials in biological applications. The as-synthesized products can be used to fabricate field-responsive photonic crystals for color display upon the application of externally applied magnetic field because of the uniform spherical structure and water dispersibility. Finally, the synthesized Fe_3O_4 nanoclusters exhibited superparamagnetic properties with high saturation magnetization and excellent magnetothermal effect, which were important for hyperthermia in biomedical applications.

Experimental

Materials

Iron (Ⅲ) chloride anhydrous ($FeCl_3$) was purchased from Xilong Chemical Co., Ltd., China. Sodium acetate anhydrous (CH_3COONa, NaAc) was obtained from Bodi Chemical Co., Ltd., China. Trisodium citrate dihydrate ($C_6H_5Na_3O_7·2H_2O$, Na_3Cit) was purchased from Dasen Chemical Product Sales Co., Ltd., China. Ethylene glycol (EG) was purchased from Fuyu Fine Chemical Co., China. Diethylene glycol (DEG) was provided by Guangfu Fine Chemical Research Institute, China. All chemicals were of analytical grade and used without further purification.

Synthesis of Fe_3O_4 nanoclusters with tunable sizes

In a typical synthetic procedure, $FeCl_3$ (10 mmol) and Na_3Cit (1 g) were dissolved in a mixed solvent of DEG and EG (total volume = 80 mL) to form a clear solution under mechanical stirring at 120 °C. After 0.5 h, NaAc (50 mmol) was added, and vigorous stirring was continued for additional 1 h. The obtained homogeneous solution was transferred to a Teflon-lined stainless steel autoclave (100 mL volume) and then sealed and heated at 200 °C. After a 10 h reaction period, the autoclave was cooled to room temperature. Dark precipitates were isolated by a magnet, washed several times with deionized water, and then dried in vacuum for 12 h.

Characterization

X-ray powder diffraction patterns (XRD) of the products were obtained on a Japan Rigaku D/Max 2400 automatic X-ray powder diffractometer equipped with graphite monochromatized Cu-Kα radiation (λ = 1.54178 Å). Scanning eletron microscopy (SEM) images were taken with a FEI Nova NanoSEM 450 apparatus. High-resolution transmission electron microscopy (HRTEM) was conducted on a FEI Tecnai G2 F30 microscope equipped with an energy-dispersive X-ray spectrometer (EDS) working at 300 kV. X-ray photoelectron spectra (XPS) were measured on a *ESCALAB250* multifunction surface analysis system using Al-Kα radiation. The average hydrodynamic sizes and zeta potential of the nanoclusters were measured on a Malvern Zetasizer Nano Series Nano-ZS90. FTIR spectroscopic analyses were conducted in transmission mode using a Thermo Scientific Nicolet 6700 FTIR spectrometer with a KBr wafer. Thermogravimetric analyses (TGA) were conducted with a TA Instruments Universal Analysis 2000. The magnetic properties (M-H curves) were measured on a Quantum Design MPMS-XL-7 system at 300 K. Digital photos of the photonic crystals were taken with a Nikon digital camera. The reflection spectra were measured using a fiber optic spectrometer (AvaSpec-2048FT-SPU, Avantes) with incident and reflection angles of 0°. The absorption measurements were conducted with a HP-8453 spectrophotometer. Magnetocaloric curves were measured on a DM100 Series Instruments for Magnetic Hyperthermia with an alternating magnetic field of Hmax =180 Gs and a fixed frequence of f=409 kHz.

Results and discussion

Monodisperse Fe_3O_4 nanoclusters were prepared by a modified solvothermal method at 200 °C via reduction of $FeCl_3$ with sodium citrate as coordinative ligand in the presence of sodium acetate as an alkali source; a mixture of DEG and EG was selected as both solvent and reductant. The growth of the Fe_3O_4 nanoclusters followed the well-documented two-stage growth model in which primary nanocrystals nucleate first in a supersaturated solution and then aggregate into larger secondary particles.[36] The mechanism underlying the synthesis of polycrystalline Fe_3O_4 nanoclusters with citrate bonding is illustrated in Scheme 1. With the formation of magnetite nanocrystals, Na_3Cit molecules were adsorbed on the surface of the nanocrystals covalently and resulted in an electrostatic repelling force between the neighboring nanocrystals. However, the surface tension of the nanocrystals made them aggregate orientedly to minimize their surface energy because of the high surface energy of the tiny nanocrystals. Once the energy barrier between the nanocrystals is achieved in the solvothermal process, a burst of a finite number of “agglomeration centers” occurs. Subsequently, the surrounding constituent subunits aggregate rapidly into clusters. Considering the process is relatively rapid, the subunits cannot take sufficient time for rearrangement. Thus, the shape of the resulting agglomerates is spherical.

Furthermore, the adsorption of citrate elevated the hydrophilic surface of Fe_3O_4 nanoclusters, making it highly water-dispersible.

---Insert Scheme 1---

The secondary structure of Fe_3O_4 nanoclusters can be observed more clearly via transmission electron microscopy (TEM). Fig. 1a reveals that the magnetite nanoclusters prepared from 1 g of Na_3Cit with V_{DEG}/V_{EG} of 40/40 exhibited a nearly uniform size of about 168 nm and a spherical shape. The selected-area electron diffraction (SAED) pattern recorded on the edge of an individual cluster reveals polycrystalline-like diffraction (Fig. 1a, inset). The diffraction spots were widened into narrow arcs that indicate slight misalignments among the primary nanocrystals, suggesting that the sphere consisted of many magnetite nanocrystals. The high-resolution TEM (HRTEM) image (Fig. 1b) further reveals that the polycrystalline structure of Fe_3O_4 nanoclusters were composed of nanocrystals with sizes of about 5.9 nm to 8.6 nm. Measuring the distance between two adjacent planes in a specific direction yielded a value of 0.48 nm, which corresponds to the lattice spacing of {111} planes of cubic magnetite (Fig. 1b, inset).

---Insert Fig. 1---

X-ray diffraction (XRD) measurements also confirmed the secondary structure of magnetite nanoclusters. Fig. 2a shows the powder XRD patterns of the products synthesized using different V_{DEG}/V_{EG} ratios. These samples exhibited similar diffraction patterns, and all the diffraction peaks can be indexed to the face-centered cubic structures of magnetite (JCPDS No. 19-0629), which agrees with the SAED pattern (Fig. 1a, inset). The broad diffraction peaks further suggested the nanocrystalline structure of the magnetite nanoclusters. The mean crystalline sizes of Fe_3O_4 primary nanocrystals were approximately 7.0, 7.9, 8.3, and 8.8 nm for the samples synthesized using 0/80, 10/70, 40/40, and 70/10 of V_{DEG}/V_{EG} respectively, which were calculated by measuring the (311) peak widths of the XRD lines in accordance with the Debye–Scherrer equation. The average sizes of these nanograins slightly increased, suggesting that variations in the V_{DEG}/V_{EG} ratio influenced the sizes of the primary nanocrystals.

Given that magnetite and maghemite (γ-Fe_2O_3) nanocrystals exhibited identical XRD patterns, X-ray photoelectron spectroscopy (XPS) was further used to distinguish Fe_3O_4 from γ-Fe_2O_3 (Fig. 2b). XPS of the products synthesized with V_{DEG}/V_{EG} of 40/40 exhibited two peaks at 710.5 and 724.4 eV, which were the characteristic peaks of Fe $2p^{3/2}$ and Fe $2p^{1/2}$ oxidation states, respectively.[37] No obvious shakeup satellite peaks (about 718.8 and 729.5 eV) existed at the high-binding-energy sides of both main peaks, which characterize Fe_3O_4.[37-39] Overall, the XRD and XPS results confirmed that the synthesized product was Fe_3O_4.

---Insert Fig. 2---

Size controllability of magnetite nanoclusters is important and may govern the fate of their applications. In this study, we designed a modified synthetic route by simply controlling the V_{DEG}/V_{EG} ratios while keeping all other parameters fixed to obtain monodispersed Fe_3O_4 nanoclusters with tunable sizes. The mean diameter of the Fe_3O_4 nanocluster products was directly proportional to the V_{DEG}/V_{EG} ratio during the solvothermal reaction. When the V_{DEG}/V_{EG} ratio varied from 0/80 to 10/70, 40/40, and 70/10, the diameters of the resulting Fe_3O_4 nanoclusters were roughly 230, 178, 168, and 94 nm, respectively (Fig. 3). The standard deviation of particle size distributions were 13.4%, 9.7%, 8.9%, and 9.2%, correspondingly, which reveals narrow size distributions (standard deviation <10%)[40,41] of the nonoclusters synthesized with the mixed-solvent system. The size of the clusters decreased with the increase in the V_{DEG}/V_{EG} ratio. However, when pure DEG was used, nonuniform small Fe_3O_4 nanoparticles were obtained with an average diameter similar to the nanocrystal size of the nanoclusters (Fig. S1†), this finding indicates that EG is essential for the synthesis of spherical Fe_3O_4 nanoparticles. Obviously, magnetite nanoparticles with regular spherical and various sizes from tens to hundreds of nanometers can be selectively obtained using this binary solvent approach. Given that DEG forms a more stable coordination complex with Fe ions than EG, the viscosity is also higher than that of EG, which led to the surface energy of the tiny nanocrystals decreased when DEG was introduced to form a binary solvent with EG. The decrease of energy barrier between the nanocrystals will result in more "agglomeration centers". Hence, the size of the Fe_3O_4 nanoclusters decreased with the increase in the V_{DEG}/V_{EG} ratio. When pure DEG was used, the Fe_3O_4 nucleates cannot agglomerate together to form large clusters because all the nanocrystals became "agglomeration centers" and only small Fe_3O_4 nanoparticles were obtained.

---Insert Fig. 3---

Additionally, Na_3Cit plays a key role in controlling the size of the Fe_3O_4 clusters in the reaction. When the initial amount of Na_3Cit increased from 0.5 g to 3.0 g, the size of the obtained magnetite particles decreased from 182 nm to 72 nm (Fig. 4), indicating that higher Na_3Cit concentration can yield magnetite nanoclusters with smaller sizes. However, excessive amount of Na_3Cit will not yield any magnetic products because the chelating ability is very strong. Few or no Na_3Cit added will lead to the production of nonuniform nanoclusters (Fig. S2†), implying that Na_3Cit acts as a morphology regulator in the system. Most importantly, the citrate can anchor on the particle surface during the solvothermal reaction, thereby enhancing the dispersibility of the magnetite clusters. Fig. 5 depicts the zeta potential of the magnetite nanoclusters synthesized with 1 g of Na_3Cit under V_{DEG}/V_{EG} of 40/40 at different pH values. The zeta potential value significantly decreased from 18.7 mV to −46.6 mV with the pH increase from 3 to 11, implying that the negative charge density on the surface of particles increased as the pH increased. This finding also suggested the existence of large amounts of carboxylate

functional groups on the magnetite particles surfaces. The schematic in Fig. 5 demonstrates the surface-state charge of Fe_3O_4 nanoclusters when the pH values were less than (i), equal (ii) and greater than (iii) the isoelectric point. Correspondingly, the effects of pH value on the particle size and polydispersity index (PDI) of Fe_3O_4 nanoclusters in the aqueous solution are summarized in Table S1†. The results showed that large aggregates existed when the pH value was near the isoelectric point for the weak electrostatic repulsion (Table S1† and Fig. 5ii). By contrast, the hydrodynamic size was nearly constant (ca. 210 nm) and the PDI was less than 0.1 when the pH value was greater than or equal to 7 (Table S1† and Fig. 5iii). The average hydrodynamic sizes of the nanoclusters were larger than their profile sizes as observed by SEM because of the thickness of the hydrated layer on the surface of clusters in water. A typical intensity particle size distribution at pH=7 (Fig. S3†) showed the narrow size distribution with a single peak and low PDI, which suggested that the Fe_3O_4 nanoclusters were monodisperse and dispersed well in water without obvious aggregation related to the strong electrostatic repulsion of the citrate.

---Insert Fig. 4---

---Insert Fig. 5---

To provide direct evidence for the presence of coordinative effect in the iron-carboxylate group, FTIR characterization was performed. Fig. S4† presents the typical FTIR spectrum of the Fe_3O_4 nanoclusters. Compared with the uncoated magnetic nanoparticles synthesized by coprecipitation (Fig. S4b†), FTIR spectra of the Fe_3O_4 nanoclusters synthesized with Na_3Cit (Fig. S4a†) exhibited not only the typical bands assigned to the Fe-O stretching at 576 cm^{-1}, but also the strong peaks at 1648 and 1400 cm^{-1}, which corresponded to $–COO^-$ antisymmetric and $–COO^-$ symmetric vibrations, indicating that numerous carboxylate groups coordinated to the Fe atom. Thermogravimetric (TG) analysis in N_2 (Fig. 6) showed distinct weight loss at the temperatures ranging from 160 °C to 400 °C; this finding was mainly attributed to the decomposition of citrate[42,43] bonded on the surface of the nanocrystals. The mass fractions of the bonded citrate calculated from Fig. 6 were 5.62%, 8.91%, and 9.52% for Fe_3O_4 nanoclusters synthesized with 0.5, 1.0, and 3.0 g of Na_3Cit, respectively. Another weight loss that occurred below 160 °C corresponded to the evaporation of the physically adsorbed water. FTIR and TG characterizations revealed that considerable amount of citrate existed in the Fe_3O_4 nanoclusters.

---Insert Fig. 6---

Magnetism is the foundation of magnetic materials. To evaluate the magnetic response of the Fe_3O_4 nanoclusters, mass magnetization for the as-obtained products was measured at room temperature (300 K) in an applied magnetic field of up to 20 k Oe. Fig. 7 shows the saturation magnetization (M_s) values of these Fe_3O_4 nanoclusters, which were determined to be 54.3, 59.0, and 68.0 emu·g^{-1} for the samples synthesized under V_{DEG}/V_{EG} of 10/70, 40/40, and 70/10, respectively. The high-saturation magnetization can be ascribed to the large sizes of the secondary structures (large clusters are constructed with tiny nanocrystals).[2,44] The small increase in the saturation magnetization value may result from the increase in the primary nanocrystal size, which was calculated using Debye–Scherrer equation. As the size of the magnetic primary nanocrystal increased, the effects of thermal agitation, surface spin-canting, and a surface magnetic dead layer became less dominant, resulting in increased magnetic properties.[33,45] Magnified hysteresis curves with magnetic field strength from −2 k Oe to 2 k Oe are also displayed as inserted in Fig. 7. The Fe_3O_4 nanoclusters demonstrated almost immeasurable coercivity and remanence, suggesting that they are superparamagnetic at room temperature. This may due to the grain size of the nanoclusters smaller than the single domain size of superparamagnetism for Fe_3O_4 (about 54 nm).[46,47] As a result, the large sized Fe_3O_4 nanoclusters still exhibited superparamagnetic property at room temperature. The superparamagnetic nature of the synthesized Fe_3O_4 nanoclusters is essential for biomedical applications, such as MRI, hyperthermia, and drug delivery, from which the materials do not retain any magnetization in the absence of an externally applied magnetic field.

---Insert Fig. 7---

The Fe_3O_4 nanoclusters were highly water-disperse and have excellent magnetic responsiveness as shown in Fig. 8a. Given the absence of an external magnetic field, the magnetite spheres were dispersed well in aqueous solution (0.04 mg·mL^{-1}). When the solution was subjected to a magnet, the nanoclusters can be completely separated from the solution within 2 min. Slight shaking will soon return the magnetite clusters into the original solution if the magnetic field was removed. Corresponding UV-Vis spectra were measured during the cycle process. Fig. 8b depicts the absorbance of the cycle process in the wavelength of 400 nm. The good collection-redispersion feature of the Fe_3O_4 nanoclusters is expected to be applied in separation technology.

---Insert Fig. 8---

These monodisperse Fe_3O_4 nanoclusters are uniformly spherical and can be well dispersed in water. Such properties are very important to obtain field-responsive colloidal photonic crystals for color display. Fig. 9 shows the digital images of the 168 nm Fe_3O_4 nanoclusters with water dispersions of about 16.3 mg·mL^{-1} in response to a varying magnetic field achieved by controlling the distance between a NdFeB magnet and the sample. The corresponding reflection spectra of the photonic crystals are show in Fig. S5†. As the magnetic field increased from 180 G to 590 G by moving the magnet toward the sample (2.6 cm to 1.5 cm), the diffraction color changed from red to blue with the corresponding diffraction peak blue-shifted from 601 nm to 439 nm. The strong diffraction color

was achieved by the balanced interactions, including the electrostatic forces of carboxylate groups and externally induced magnetic forces. Blue-shift of the peak wavelength was due to the decrease of the interparticle distance as the magnetic field increased by moving the magnet toward the sample, which can be explained by Bragg's Law ($m\lambda = 2nd\sin\theta$; m is the order of scattering, λ is the diffraction wavelength, n is the refractive index of water, d is the interparticle distance, and θ is the angle between the incident light and the diffraction crystal plane).[48] However, other samples with too large or too small diameters can not exhibit diffraction light covering the whole visible spectrum.[24] The optical response of these photonic crystals to external magnetic stimuli is relatively rapid, which is a critical feature for the potential application in the field of magnetic responsive display.

---Insert Fig. 9---

Magnetocaloric property is another vital feature of magnetic materials, making them among the most feasible candidates for hyperthermia and controlled drug release. In this study, the magnetothermal effect of the Fe_3O_4 nanoclusters was investigated with a instrument for magnetic hyperthermia (Fig. 10). Obviously, the heating rate accelerated with the increase of the nanoclusters' concentration in aqueous solution (Fig. 10a). Up to 20 mg·mL^{-1} of magnetite nanoclusters (168 nm) can increase to about 74.4 °C from 27.7 °C within 242 s, indicating that the products we synthesized exerted an excellent magnetothermal effect. The influence of cluster size on the heating rate was also studied (Fig. 10b). The heating rate increased with the decrease in the size, which probably contributed to the increase in the saturation magnetization.

---Insert Fig. 10---

Conclusions

We developed a simple solvothermal approach to synthesize highly water-dispersible superparamagnetic Fe_3O_4 particles with tunable uniform sizes by using sodium citrate with a mixed-solvent system of DEG/EG. The diameters of the Fe_3O_4 nanoparticles can be effectively adjusted from tens to hundreds of nanometers by varying the volume ratio of DEG/EG. Moreover, owing to the presence of the citrate attached on the surface, the Fe_3O_4 particles demonstrated excellent water dispersibility and dispersing stability. The synthesized Fe_3O_4 nanoclusters presented high-saturation magnetization of up to 68.0 emu·g^{-1} and exhibited superparamagnetism at room temperature, thereby enhancing their response to the external magnetic field. These monodisperse Fe_3O_4 nanoclusters can be well dispersed in water and diffract color under visible light upon the application of an externally applied magnetic field, which can be used to construct field-responsive colloidal photonic crystals for color display. Furthermore, these biocompatible Fe_3O_4 nanoclusters can be applied to hyperthermia in biomedical applications because of the excellent magnetothermal effects. Overall, these highly water-dispersible and citrate-functionalized superparamagnetic magnetite nanoclusters with high magnetization and tunable sizes will be promising in optics and biomedical applications.

Acknowledgements

This work was supported by the National Natural Science Foundation of China (21276042, 21421005), the National Science and Technology Pillar Program (2013BAF08B06), Program for Innovative Research Team in University (IRT_13R06).Fundamental Research Funds for the Central Universities (DUT13LK35 , DUT14YQ209, DUT2013TB07, DUT14QY13), Program for New Century Excellent Talents in University (NCET130080). Program for Liaoning Excellent Talents in University (LJQ2013006).

Notes and references

1 D. B. Wang, C. X. Song, Y. H. Zhao and M. L. Yang, *J. Phys. Chem. C*, 2008, **112**, 12710.
2 Y. F. Zhu, W. R. Zhao, H. R. Chen and J. L. Shi, *J. Phys. Chem. C* , 2007**, 111**, 5281.
3 A. G. Hu, G. T. Yee and W. B. Lin, *J. Am. Chem. Soc.*, 2005, **127**, 12486.
4 T. Hyeon, *Chem. Commun.*, 2003, 927.
5 A.-H. Lu, W. Schmidt, N. Matoussevitch, H. Bönnermann, B. Spliethoff, B. Tesche, E. Bill, W. Kiefer and F. Schüth, *Angew. Chem. Int. Ed.*, 2004, **43**, 4303.
6 S. Mornet, S. Vasseur, F. Grasset and E. Duguet, *J. Mater. Chem.*, 2004, **14**, 2161.
7 F. Q. Hu, L. Wei, Z. Zhou, Y. L. Ran, Z. Li and M. Y. Gao, *Adv. Mater.*, 2006, **18**, 2553.
8 M. Shokouhimehr, Y. Z. Piao, J. Kim, Y. J. Jang and T. Hyeon, *Angew. Chem. Int. Ed.*, 2007**, 119**, 7169.
9 S. H. Sun and H. Zeng, *J. Am. Chem. Soc.*, 2002, **124**, 8204.
10 S. H. Xuan, F. Wang, J. M. Y. Lai, K. W. Y. Sham, Y.-X. J. Wang, S.-F. Lee, J. C. Yu, C. H. K. Cheng and K. C.-F. Leung, *ACS Appl. Mater. Interfaces*, 2011, **3**, 237.
11 T. Hyeon, S. S. Lee, J. Park, Y. Chung and H. B. Na, *J. Am. Chem. Soc.*, 2001, **123**, 12798.
12 F. L. Sousa, R. Bustamante, A. Millan, F. Palacio, T. Trindade and N. J. O. Silva, *Nanoscale*, 2013, **5**, 7229.
13 A. P. Zhu, L. H. Yuan, W. J. Jin, S. Dai, Q. Q. Wang, Z. F. Xue and A. J. Qin, *Acta Biomater.*, 2009, **5**, 1489.
14 M. C. Cai, H. Qian, Z. K. Wei, J. J. Chen, M. S. Zheng and Q. F. Dong, *RSC Adv.*, 2014, **4**, 6379.
15 J. S. Zhou, H. H. Song, L. L. Ma and X. H. Chen, *RSC Adv.*, 2011, **1**, 782.
16 T. Q. Wang, X. L. Wang, Y. Lu, Q. O. Xiong, X. Y. Zhao, J. B. Cai, S. Huang, C. D. Gu and J. P. Tu, *RSC Adv.*, 2014, **4**, 322.
17 R. Hao, R. J. Xing, Z. C. Xu, Y. L. Hou, S. Gao and S. H. Sun, *Adv. Mater.*, 2010, **22**, 2729.
18 S. Laurent, D. Forge, M. Port, A. Roch, C. Robic, L. V. Elst, R. N. Muller, *Chem. Rev.*, 2008, **108**, 2064.
19 S. Shen, F. F. Kong, X. M. Guo, L. Wu, H. J. Shen, M. Xie, X. S. Wang, Y. Jin and Y. R. Ge, *Nanoscale*, 2013, **5**, 8056.
20 Y.-K. Choi, D. H. Lee, Y.-K. Seo, H. Jung, J.-K. Park and H. Cho, *Appl. Biochem. Biotechnol.*, 2014, **174**, 1233.
21 H. Kim, J. P. Ge, J. Kim, S.-e. Choi, H. Lee, H. Lee, W. Park, Y. D. Yin, S. Kwon, *Nat. Photonics*, 2009, **3**, 534.
22 X. M. Wang, H. C. Gu, Z. Q. Yang, *J. Magn. Magn. Mater.*, 2005, **293**, 334.

23 J. B. Li, Y. Qu, J. Ren, W. Z. Yuan and D. L. Shi, *Nanotechnology*, 2012, **23**, 1.
24 J. P. Ge, Y. X. Hu and Y. D. Yin, *Angew. Chem.*, 2007, **119**, 7572.
25 L. Lartigue, C. Innocenti, T. Kalaivani, A. Awwad, M. d. M. Sanchez Duque, Y. Guari, J. Larionova, C. Guérin, J.-L. G. Montero, V. Barragan-Montero, P. Arosio, A. Lascialfari, D. Gatteschi and C. Sangregorio, *J. Am. Chem. Soc.*, 2011, **133**, 10459.
26 Y. X. Hu, L. He and Y. D. Yin, *Angew. Chem. Int. Ed.*, 2011, **50**, 3747.
27 R. Zhao, K. Jia, J. J. Wei, J. X. Pu, X. B. Liu, *Mater. Lett.*, 2010, **64**, 457.
28 S. H. Gee, Y. K. Hong, D. W. Erickson, M. H. Park and J. C. Sur, *J. Appl. Phys.*, 2003, **93**, 7560.
29 S. H. Xuan, F.Wang, Y.-X. J. Wang, J. C. Yu and K. C.-F. Leung, *J. Mater. Chem.*, 2010, **20**, 5086.
30 J. Liu, Z. K. Sun, Y. H. Deng, Y. Zou, C. Y. Li, X. H. Guo, L. Q. Xiong, Y. Gao, F. Y. Li and D. Y. Zhao, *Angew. Chem. Int. Ed.*, 2009, **121**, 5989.
31 H. Deng, X. L. Li, Q. Peng, X. Wang, J. P. Chen and Y. D. Li, *Angew. Chem.*, 2005, **117**, 2842.
32 J. P. Ge, Y. X. Hu, M. Biasini, W. P. Beyermann and Y. D. Yin, *Angew. Chem. Int. Ed.*, 2007, **46**, 4342.
33 J. N. Gao, X. Z. Ran, C. M. Shi, H. M. Cheng, T. M. Cheng and Y. P. Su, *Nanoscale*, 2013, **5**, 7026.
34 S. H. Xuan, Y.-X. J. Wang, J. C. Yu, K. C.-F. Leung, *Chem. Mater.*, 2009, **21**, 5079.
35 L. Zhang, R. He and H. C. Gu, *Appl. Surf. Sci.*, 2006, **253**, 2611.
36 X. L. Hu, J. M. Gong, L. Z. Zhang and J. C. Yu, *Adv. Mater.*, 2008, **20**, 4845.
37 T. Yamashita and P. Hayes, *Appl. Surf. Sci.*, 2008, **254**, 2441.
38 Y. B. Liu, Y. Q. Wang, S. M. Zhou, S. Y. Lou, L. Yuan, T. Gao, X. P. Wu, X. J. Shi and K. Wang, *ACS Appl. Mater. Interfaces*, 2012, **4**, 4913.
39 Q. Gao, F. H. Chen, J. L. Zhang, G. Y. Hong, J. Z. Ni, X. Wei and D. J. Wang, *J. Magn. Magn. Mater.*, 2009, **321**, 1052.
40 S. J. Guo and E. K. Wang, *Inorg., Chem.*, 2007, **46**, 6740.
41 Y. G. Sun, S. K. Gray and S. Peng, *Phys. Chem. Chem. Phys.*, 2011, **13**, 11814.
42 C. M. Cheng, Y. H. Wen, X. F. Xu and H. C. Gu, *J. Mater. Chem.*, 2009, **19**, 8782.
43 J. H. Park, J. P. Kim, H. T. Kwon and J. Kim, *Desalination*, 2008, **233**, 73.
44 Y. L. Liu, C. M. Li, H. T. Zhang, X. L. Fan, Y. Liu and Q. Y. Zhang, *Chem. Eng. J.*, 2015, **259**, 779.
45 J. M. D. Coey, *Phys. Rev. Lett.*, 1971, **27**, 1140.
46 A. Aharoni and J. P. Jakubovics, *IEEE Trans. Magn.*, 1988, **24**, 1892.
47 Y. H. Zheng, Y. Cheng, F. Bao and Y. S. Wang, *Mater. Res. Bull.*, 2006, **41**, 525.
48 H. B. Hu, C. L. Chen and Q. W. Chen, *J. Mater. Chem. C*, 2013, **1**, 6013.

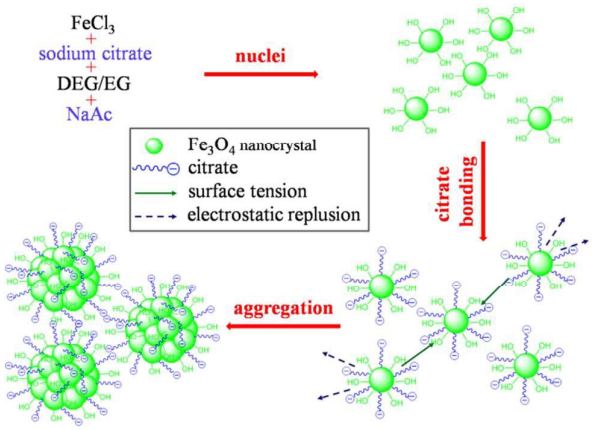

Scheme 1 Schematic illustration showing the formation of citrate-functionalized Fe_3O_4 nanoclusters.

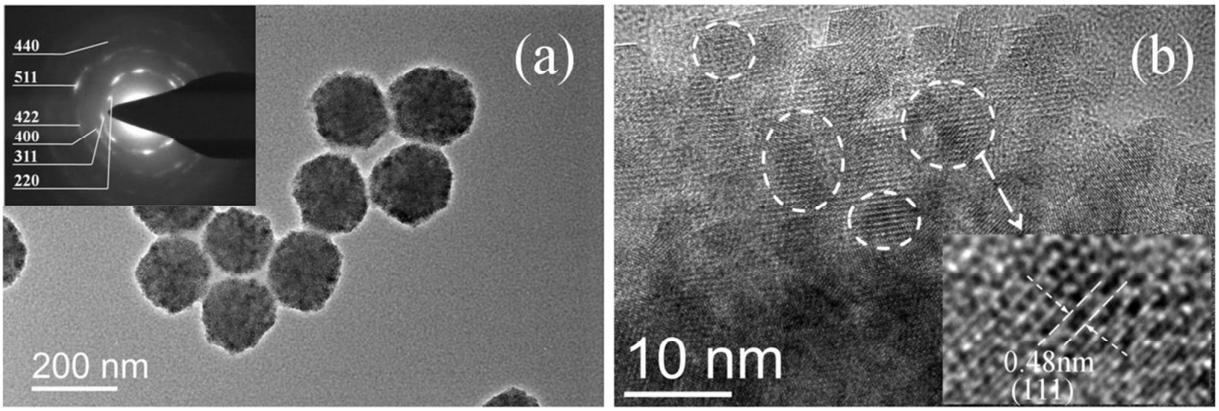

Fig. 1 (a) TEM images of 168 nm Fe_3O_4 nanoclusters and SAED pattern (inset), (b) HRTEM image of the cluster in (a).

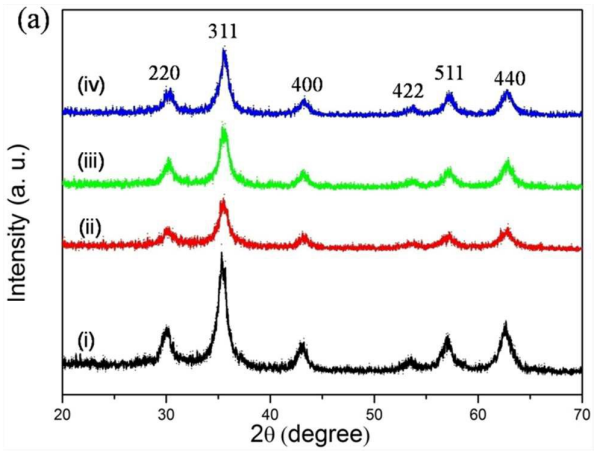

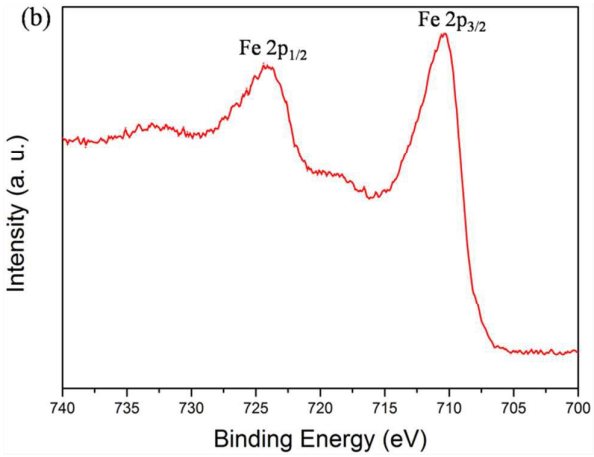

Fig. 2 (a) XRD patterns of the Fe_3O_4 nanoclusters which were synthesized by using different ratios of V_{DEG} /V_{EG}: (i) 0/80, (ii) 10/70, (iii) 40/40 and (iv) 70/10; and (b) X-ray photoelectron spectrum (XPS) of Fe_3O_4 nanoclusters synthesized with 1 g Na_3Cit under V_{DEG} /V_{EG} =40/40.

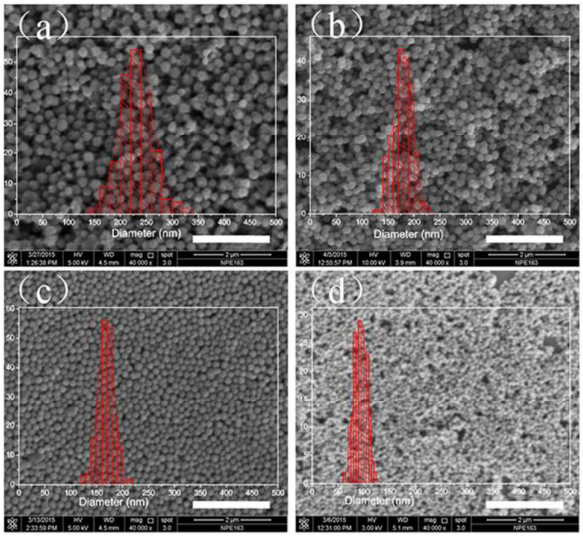

Fig. 3 SEM images and the particle size distribution of Fe_3O_4 nanoclusters synthesized with different ratio of V_{DEG} /V_{EG}: （a）0/80, (b) 10/70, (c) 40/40 and (d) 70/10. Scale bars: 2 um.

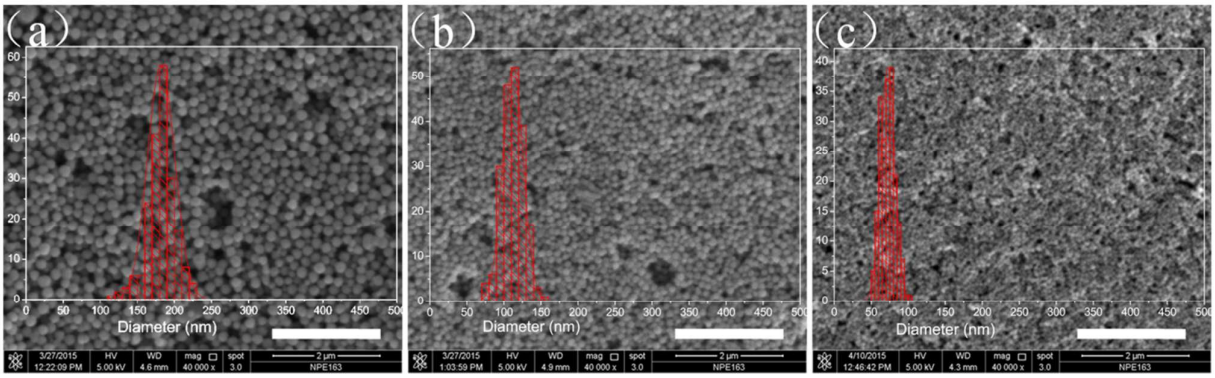

Fig. 4 SEM images and the particle size distribution of Fe_3O_4 nanoclusters synthesized with different dosage of Na_3Cit: (a)0.5, (b) 1.5 and (c) 3 g. Scale bars: 2 um.

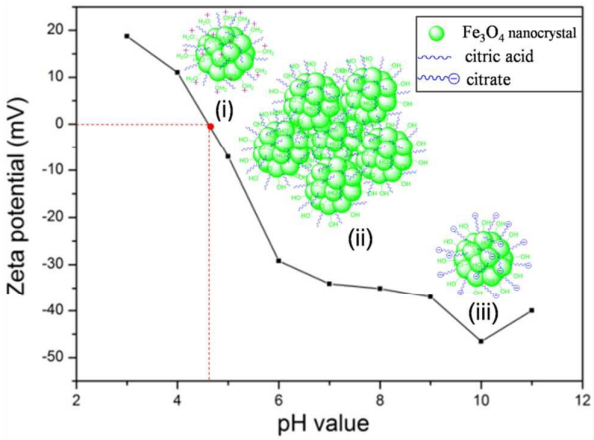

Fig. 5 Zeta potential of Fe_3O_4 nanoclusters water dispersions synthesized with 1 g Na_3Cit under V_{DEG} /V_{EG} =40/40 at different pHs and schematic representation of the surface charge state when pH value less than (i), equal (ii) and greater than (iii) the isoelectric point (red point).

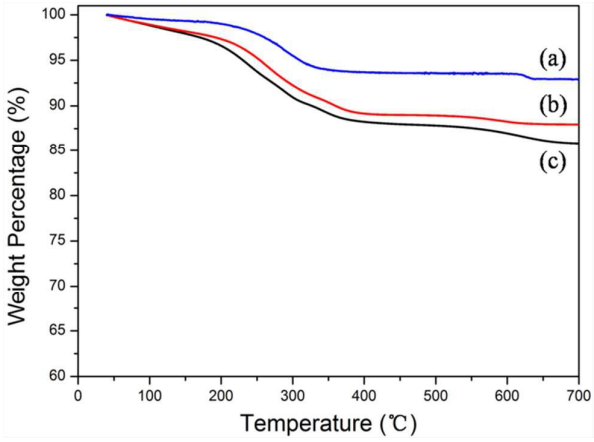

Fig. 6 Thermogravimetric (TG) curves of Fe_3O_4 nanoclusters synthesized with different dosage of Na_3Cit: (a) 0.5, (b) 1 and (c) 3g.

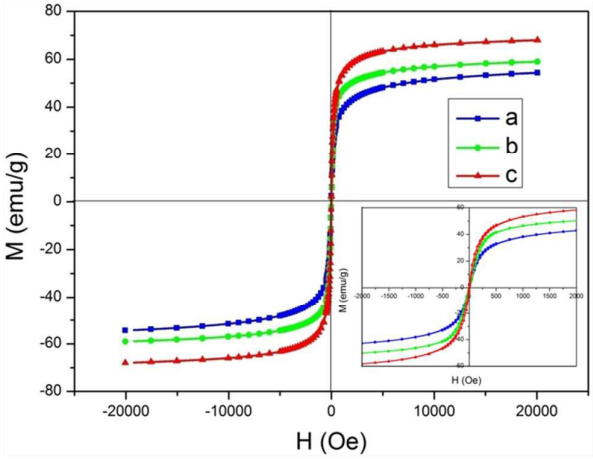

Fig. 7 Magnetization loops for Fe_3O_4 nanoclusters synthesized by using different ratios of V_{DEG} /V_{EG}: (a) 10/70, (b) 40/40 and (c) 70/10 at room temperature. The inset shows the respective expanded plots for field between −2k and 2k Oe.

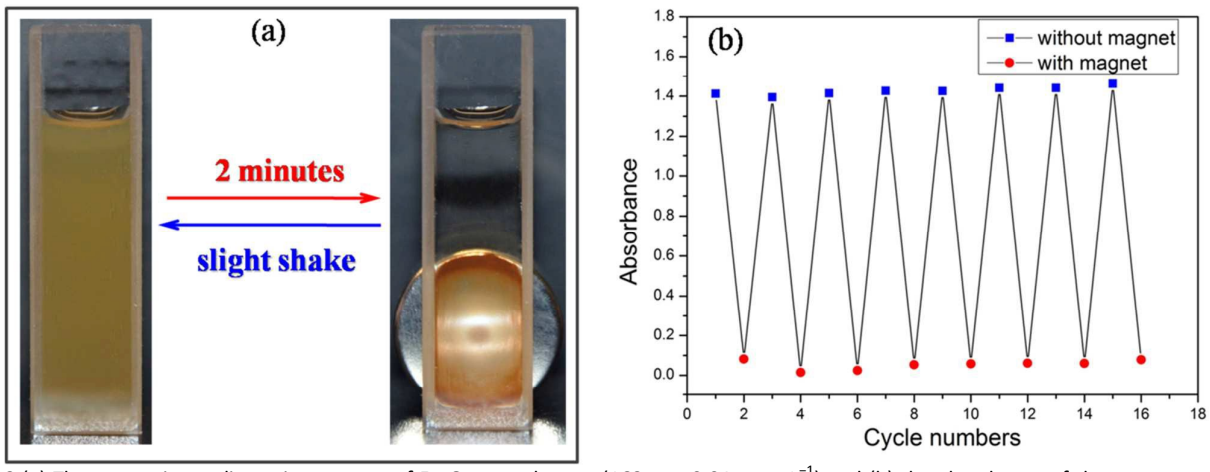

Fig. 8 (a) The separation-redispersion process of Fe_3O_4 nanoclusters (168 nm, 0.04 mg·mL^{-1}) and (b) the absorbance of the corresponding cycle process in the wavelength of 400 nm by UV-Vis spectrum.

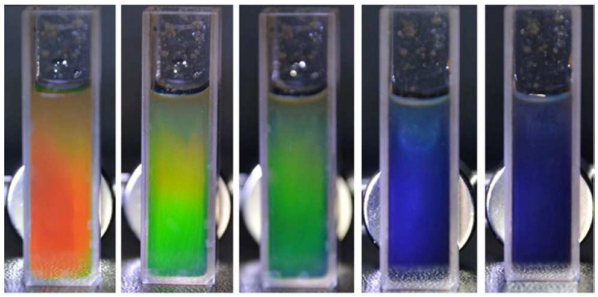

Fig. 9 Digital photos of the photonic crystals formed in response to an external magnetic field with the 168 nm Fe_3O_4 nanoclusters (ca. 16.3 mg·mL^{-1}), the magnet–sample distance decreases gradually from left to right.

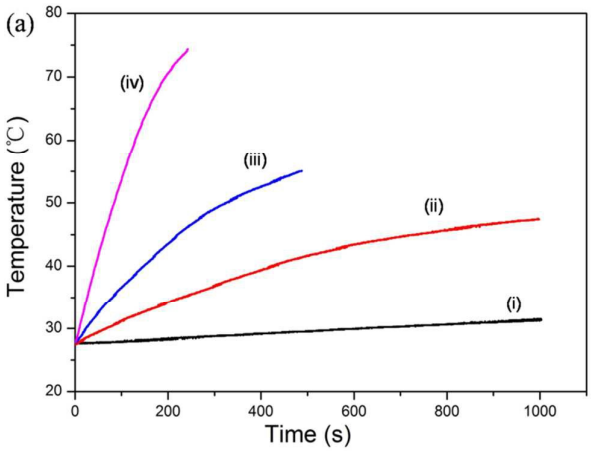

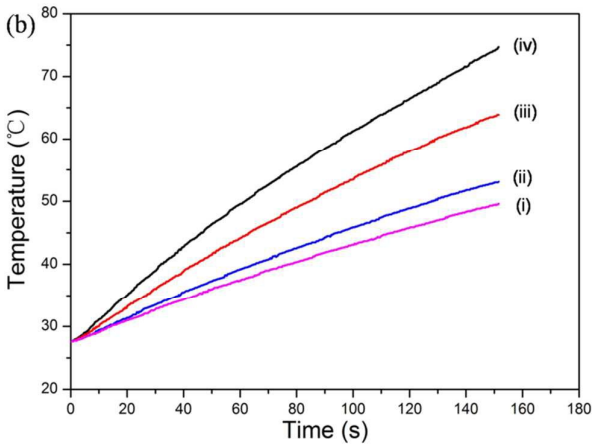

Fig. 10 (a) Magnetocaloric curves of Fe_3O_4 nanoclusters (168 nm) aqueous solution with different concentration: (i) 1, (ii) 5, (iii) 10 and (iv) 20 mg·mL^{-1} and (b) magnetocaloric curves of 20 mg·mL^{-1} Fe_3O_4 nanoclusters aqueous solution with different sizes: (i) 230, (ii) 178, (iii) 168 and (iv) 94 nm in an alternating magnetic field.

Table of Contents (TOC) Entry:

Synthesis of citrate grafted superparamagnetic Fe_3O_4 nanoclusters with tunable size by varying the volume ratio of DEG/EG.